National University of Skill

Visual Journal of Technical and Vocational Education

Volume 3, Issue 2
2026, Pages XXX–XXX
ISSN: [3060-6357]

RESEARCH ARTICLE

Effects of Pin Geometry and Processing Parameters on Macroscopic Defects in Three-Layer Friction Stir Additive Manufacturing of AA7075

Mostafa Akbari[1*], **Ezatollah Hassanzadeh**[2], **Amirhossein Sardarizadeh**[3,]

[1,2,3] Department of Mechanical Engineering, Technical and Vocational University (TVU), Tehran, Iran.
* Corresponding author. Email: mr.mostafaakbari@yahoo.com

ARTICLE INFO

Keywords

Friction stir additive manufacturing
AA7075
Pin geometry
Pin length
Macroscopic defects

ABSTRACT

Friction stir additive manufacturing (FSAM) relies on local softening, material transport, and interfacial consolidation to join successive metal sheets. This study examines macroscopic discontinuities and defects in three-layer AA7075 builds produced from nominally 1.6 mm sheets through two joining stages. Twenty selected combinations of conical, cylindrical, and threaded pins, 2 and 3 mm pin lengths, rotational speeds of 2000 and 3150 rpm, and traverse speeds of 36 and 45 mm/min were assessed using cross-sectional photographs. Visible discontinuity areas ranged from 0.08 to 2.09 mm² in the sections containing resolved defects. Sections with no detectable macroscopic discontinuity (ND) were assigned zero for all comparative means. Threaded pins gave the lowest pooled mean discontinuity area, 0.334 mm², and the threaded 2 mm tool at 45 mm/min produced ND sections at both rotational speeds. Comparisons at otherwise identical settings showed that changing traverse speed, rotation, or pin length could improve or impair consolidation depending on the accompanying tool geometry. These responses are interpreted in terms of geometry-dependent stirring, interlayer engagement, and the balance between thermal softening and material containment. The results identify favorable tested combinations and indicate that pin profile and processing speeds should be selected together to promote interlayer filling and closure.

1. Introduction

The demand for lightweight structural components has encouraged manufacturing approaches that combine the specific strength of aluminium alloys with reliable joining and controlled material consolidation. AA7075 is an attractive candidate for such applications, but processing high-strength, heat-treatable aluminium requires careful management of both bonding and thermal exposure. Conventional fusion joining can be difficult for aerospace aluminium alloys, whereas friction stir welding (FSW) provides a solid-state route in which deformation and frictional heating establish a joint without bulk melting [1, 2].

Friction stir additive manufacturing (FSAM) applies this joining principle to a layered build [3, 4]. In the sheet-based configuration, a non-consumable rotating tool traverses overlapping sheets, consolidating an added sheet with the underlying material; further sheets are subsequently placed and joined to increase the build height [5, 6]. The shoulder and pin create a coupled thermal and deformation field, making the tool configuration central to interlayer bonding [7]. Mishra et al. [8] distinguished sheet-based FSAM from additive friction stir deposition (AFSD), which introduces feedstock through a different deposition arrangement. This distinction matters when interpreting published parameter windows: results obtained with a continuous feedstock deposition system cannot be transferred directly to a stacked-sheet process. Although both approaches avoid a melting and solidification cycle, their material flow and boundary conditions differ.

Avoiding solidification does not ensure complete consolidation. The FSAM review by Hassan et al. [3] identified hooks, weak or kissing bonds, voids, cavities, and tunnels among the discontinuities reported in layered builds. These features reflect different combinations of interfacial deformation, local material transport, and tool engagement. A visible cavity indicates an open discontinuity, whereas an interface with weak bonding may remain difficult to distinguish in a macroscopic section. Consequently, assessing the occurrence and extent of visible defects is an important part of developing an FSAM process. The relevant process window must therefore be evaluated using clearly defined observations and measurement criteria.

The existing literature establishes that AA7075 can be manufactured by FSAM and that tool design, processing speeds, pass history, and thermal management influence the resulting build. The present study addresses visible discontinuities in thin AA7075 sheets consolidated through a three-layer sequence. Twenty tested combinations of pin geometry, pin length, rotational speed, and traverse speed are compared using the total visible discontinuity area in each examined section. Particular attention is given to comparisons at otherwise identical settings and to the relationship between pin engagement, material transport, and thermal softening. This assessment identifies favorable tested conditions for interlayer closure while retaining a clear distinction between a resolved cavity and a section with no clearly detectable macroscopic discontinuity.

2. Literature review

Early experimental work already demonstrated the close connection between additive consolidation and processing conditions. Palanivel et al. [9] fabricated multilayer WE43 magnesium alloy stacks and examined defects, interfacial microstructure, and mechanical behaviour. Defect formation was sensitive to the applied heat input, while deformation-induced grain refinement and precipitation

characteristics contributed to the resulting structural performance. This study showed that the value of FSAM depends on how successfully the material is consolidated as well as on the microstructure produced. Its results provide a process-level precedent for studying defects, although the magnesium alloy and experimental configuration differ from those of an AA7075 sheet stack.

For aluminium builds, Mao et al. [10] investigated formation characteristics, microstructure, and mechanical performance in a multilayer FSAM component. They observed that hook geometry changed as subsequent layers were added: material extruded during the next joining step altered the orientation of interfaces created previously. Grain structure, precipitate characteristics, and hardness also varied along the build direction. These observations are particularly relevant to sequential sheet addition because a joining operation can affect material that has already undergone a preceding pass. The final cross-section thus records the interaction of successive operations rather than only the conditions experienced by the most recently added sheet.

The influence of successive thermal and deformation histories has also been addressed through modelling and experiments. Zhang et al. [11] integrated thermal calculations, grain evolution, precipitation behaviour, and property prediction in an FSAM process–microstructure–property framework. Their work linked reheating and renewed stirring to variations along the building direction and identified layer thickness as a relevant processing variable. In a three-layer, sheet-based AA6061 build, Han et al. [12] found differences between the central regions of individual layers and the underlying thermomechanically affected zones. Grain refinement coexisted with no uniform hardness and layer-dependent mechanical behaviour. Together, these studies show that a successfully formed multilayer structure need not have uniform properties, and that consolidation quality and subsequent material performance require separate consideration.

Direct investigations of AA7075 have emphasized the importance of pin geometry. Hassan et al. [13] compared plain cylindrical, cylindrical threaded, and taper threaded pins in four-layer laminates at different rotational and traverse speeds. Within their tested conditions, the taper-threaded pin produced laminates reported as free of defects, and the authors also documented changes in grain size and microhardness. The result demonstrates that pin profile can materially alter the effectiveness of a given parameter combination. It does not establish a universal ranking of pin shapes, because tool dimensions, sheet thickness, engagement, and the applied speeds determine the particular flow conditions.

Parameter selection for AA7075 has subsequently been investigated through broader performance objectives. Hassan et al. [14] produced seven-layer laminates under forced cooling and used a Taguchi design with grey relational analysis to consider stirring speed, welding speed, and the number of passes in relation to hardness, ultimate tensile strength, and elongation. This approach illustrates why processing conditions can require simultaneous evaluation against several responses.

Recent work by Girish [15] on a double-layer AA7075 FSAM build reported a macroscopically sound, basin-shaped consolidated region together with variations in grain size and hardness through its thickness. The study further demonstrates the coexistence of apparently successful consolidation and a heterogeneous material state.

3. Materials and methods

3.1. Materials and sequential sheet joining

Friction stir additive manufacturing (FSAM) builds layered components by sequentially adding and friction stir joining metal sheets. During joining, a rotating tool is brought into contact with the upper sheet and traversed along the joining path. Frictional heating and deformation promote local material flow, while the pin stirs material across the sheet interface and the shoulder contributes to surface contact and consolidation [16]. Repetition of this solid-state joining operation produces the layered build. The starting material was AA7075 aluminium sheet with a nominal thickness of 1.6 mm. Nominal chemical composition limits for AA7075 are summarized in Table 1.

Three sheets were joined in two successive stages, as illustrated in Fig. 1. Sheets 1 and 2 were first stacked and friction stir welded to form a two-layer assembly. Sheet 3 was subsequently placed on top of this assembly and joined in a second stage. The final build therefore comprised three sheets and two interlayer joining stages. Joining was performed using a milling machine.

Table 1. chemical composition of AA7075 (wt.%; balance Al).

Alloy	Al	Zn	Mg	Cu	Cr	Fe	Si	Mn	Ti
AA7075	Bal.	6.1	2.3	1.4	0.19	≤0.50	≤0.40	≤0.30	≤0.20

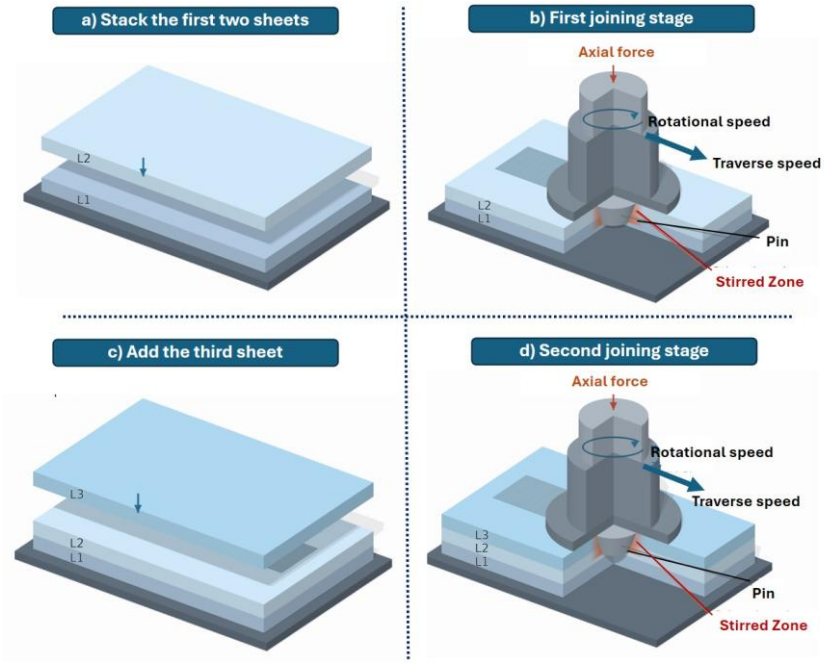


Fig. 1. Sequential FSAM of three AA7075 sheets: (a) stacking sheets 1 and 2; (b) first joining stage; (c) adding sheet 3; and (d) second joining stage.

3.2. Tool geometries and processing parameters

Three pin geometries were investigated: conical, cylindrical, and threaded (Fig. 2). The tools were manufactured from H13 tool steel and hardened before joining. The conical tool had a shoulder diameter of 18 mm and a pin root diameter of 6 mm. The cylindrical and threaded pins had a diameter of 6 mm. Pin length was varied between 2 and 3 mm. A tool tilt angle of 3° and a steel backing plate were used during joining.

The processing conditions and associated discontinuity-area estimates are listed in Table 2. Rotational speeds of 2000 and 3150 rpm and traverse speeds of 36 and 45 mm/min were investigated with the three pin profiles and two pin lengths. Each listed parameter combination was used for both joining stages. Twenty selected conditions were examined. Samples 1–8 used conical pins, samples 9–15 cylindrical pins, and samples 16–20 threaded pins. ND denotes no clearly resolved macroscopic discontinuity in the examined field and is assigned 0.00 mm² for comparisons.

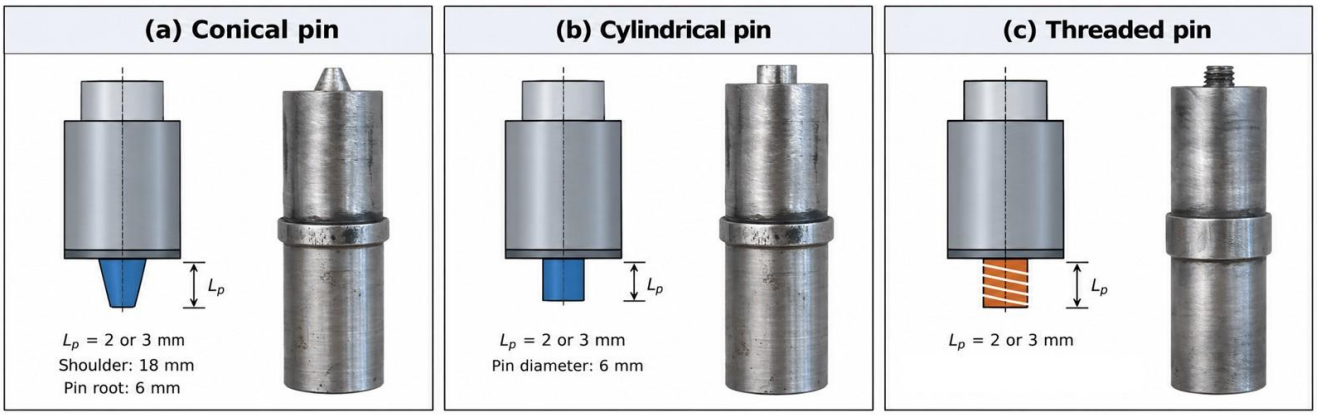


Fig. 2. Tool pin profiles: (a) conical, (b) cylindrical, and (c) threaded.

Sample ID	Pin geometry	Traverse speed (mm/min)	Rotational speed (rpm)	Pin length (mm)	Discontinuity area (mm², ND = 0)
1	Conical	36	3150	3	0.48
2	Conical	45	2000	3	0.98
3	Conical	45	2000	2	0.08
4	Conical	36	3150	2	1.74
5	Conical	36	2000	2	0.17
6	Conical	45	3150	3	2.09
7	Conical	36	2000	3	0.17
8	Conical	45	3150	2	0.00 (ND)
9	Cylindrical	45	3150	3	0.14
10	Cylindrical	36	3150	3	0.91
11	Cylindrical	45	2000	3	0.76
12	Cylindrical	36	3150	2	1.14
13	Cylindrical	45	3150	2	0.66
14	Cylindrical	36	2000	2	0.78
15	Cylindrical	36	2000	3	0.00 (ND)
16	Threaded	36	3150	3	0.17
17	Threaded	36	3150	2	1.00
18	Threaded	36	2000	2	0.50
19	Threaded	45	2000	2	0.00 (ND)
20	Threaded	45	3150	2	0.00 (ND)

Table 2. Processing conditions and visible discontinuity areas, grouped by pin geometry. Each row applies to both joining stages; ND sections are assigned 0.00 mm².

3.3. Macroscopic examination and defect-area assessment

After joining, sections were prepared by abrasive grinding and photographed using a stereomicroscope. Visible cavities and open discontinuities were assessed by Python-based image analysis of the original photographs before display resampling or sharpening. Image intensity was calculated as the mean of the three 8-bit color channels. Features were segmented within reviewed regions using sample-specific intensity thresholds of 60–100, followed by binary closing with a 3 × 3 pixel structuring element and hole filling. Components smaller than approximately 0.0019 mm² were excluded, and long, thin preparation-mark fragments were rejected in affected clustered regions. Selected pixel counts were converted to two-dimensional discontinuity areas using the image scales. The boundary-connected opening in sample 14 was included within the examined field. Fig. 3 presents the assessed sections in the sample-number sequence listed in Table 2.

ND sections were retained as observations with no clearly resolved macroscopic cavity and assigned zero area for every comparative calculation. Reported areas describe visible two-dimensional discontinuities in the examined field.

3.4. Comparison of processing conditions

The response is the total estimated visible discontinuity area in each section, expressed in mm². All group means use ND = 0: areas, including assigned zeros, are summed and divided by the number of examined sections in the group. Means are calculated from the two-decimal areas in Table 2. Comparisons at otherwise identical settings are used to discuss the effects of pin geometry, rotation, traverse speed, and pin length in terms of established flow and heating mechanisms.

4. Results

4.1. Defect morphology and interlayer closure

Fig. 3 compares cavity clusters, irregular voids, and an extended opening. Samples 1, 9, 10, 16, 17, and 18 show localized clusters; samples 2, 4, 6, 11, 12, and 13 contain prominent cavities. Sample 3 has a small isolated cavity, and samples 5 and 7 show limited discontinuities. Sample 14 contains an extended opening connected to the image boundary. Samples 8, 15, 19, and 20 have no clearly resolved macroscopic cavity and receive zero area under ND = 0.

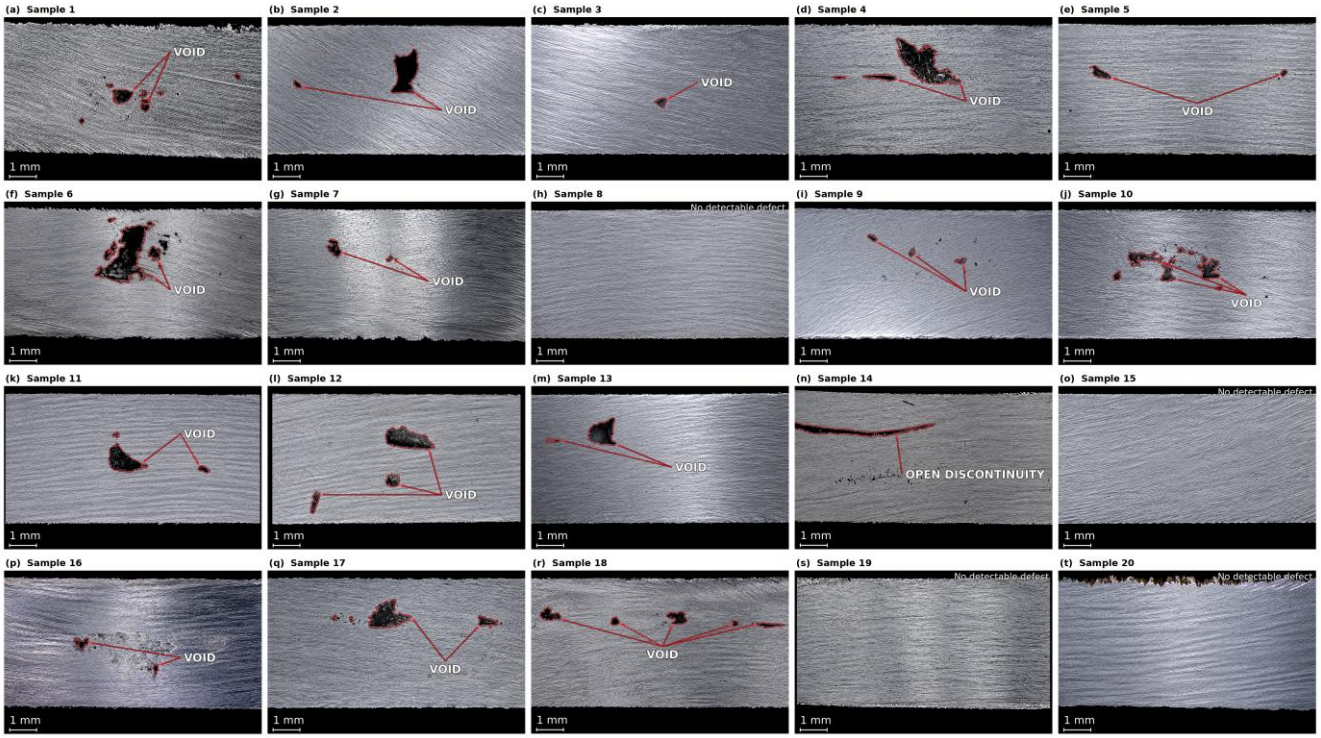


Fig. 3. Macroscopic sections of the samples listed in Table 2. Panels (a–t) correspond to samples 1–20, respectively. Red outlines and arrows mark visible voids and the open discontinuity. All panels use the same physical magnification; scale bars represent 1 mm. ND denotes no clearly resolved macroscopic discontinuity.

4.2. Overview of the tested conditions

Table 3 and Fig. 4 summarize the tested conditions. The lowest pooled means occur for threaded pins, 2000 rpm, 45 mm/min, and 2 mm pin length. Each mean describes the parameter combinations tested in that group and is interpreted alongside the flow and heating mechanisms discussed below. The different responses across pin profiles indicate that material engagement and thermomechanical conditions should be considered together.

Parameter	Level	Mean discontinuity area (mm^2, ND = 0)
Pin geometry	Conical	0.714
Pin geometry	Cylindrical	0.627
Pin geometry	Threaded	0.334
Rotational speed	2000 rpm	0.382
Rotational speed	3150 rpm	0.757
Traverse speed	36 mm/min	0.642
Traverse speed	45 mm/min	0.523
Pin length	2 mm	0.552
Pin length	3 mm	0.633

Table 3. Mean visible discontinuity area, including every examined section in the corresponding tested group.

5. Discussion

Such morphology is consistent with incomplete local filling or closure during friction-stir consolidation. Material displaced around the tool must be transferred into the region behind it and compressed into a continuous joint. Local softening assists this transport, while shoulder contact supplies containment and forging action [7, 16]. A cavity can consequently remain when the delivered material and closure conditions do not match the space created by the moving tool. In the present two-stage build, the second joining operation also reheats and deforms part of the previously consolidated assembly; the final section reflects this cumulative processing history [10, 11]. The following mechanisms are interpretations of the observed sections rather than directly measured flow paths or temperatures.

5.1. Pin geometry and material transport

Pin geometry determines how softened material is displaced circumferentially and exchanged through the sheet interface. A smooth cylindrical pin maintains approximately the same radius along its body, whereas the radius of a conical pin decreases toward the tip. At a fixed angular speed, the local tool-surface velocity therefore decreases with depth along a conical pin. The resulting contact and deformation fields differ from those of a cylindrical pin, even when their root diameters and nominal lengths are similar. Threads introduce a helical contact feature that can promote axial exchange together with circumferential stirring [7, 16]. Thread handedness and rotation determine the direction of this helical transport.

The pooled means are 0.334 mm^2 for threaded, 0.627 mm^2 for cylindrical and 0.714 mm^2 for conical pins. The threaded mean is approximately 53.2% below the conical and 46.7% below the cylindrical mean. Threaded pins include two ND sections among five conditions, compared with one among seven cylindrical and one among eight conical conditions.

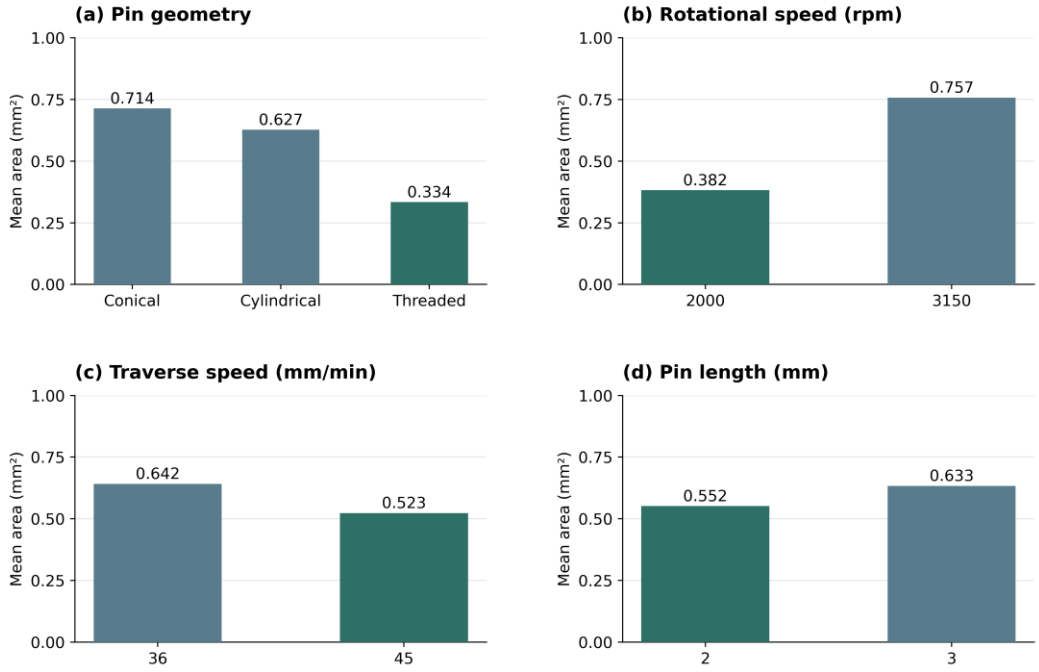


Fig. 4. Mean visible discontinuity area under ND = 0, grouped by (a) pin geometry, (b) rotational speed, (c) traverse speed, and (d) pin length. Means include ND sections assigned zero.

5.2. Traverse speed and local thermal exposure

Traverse speed sets the time during which a material region remains under the moving tool. Increasing travel speed reduces local residence time and, for comparable mechanical power, decreases the energy supplied per unit length. A slower pass provides more time for softening and redistribution, but stronger softening also changes the resistance of the material to displacement and the demand for effective shoulder containment. Conversely, a faster pass can shorten the time available to transfer material across the interface. The favorable travel speed thus depends on whether the selected pin produces adequate transport and closure within that thermal and deformation window [16, 17].

The pooled mean area is 0.642 mm² at 36 mm/min and 0.523 mm² at 45 mm/min. Increasing traverse speed therefore corresponds to an approximately 18.5% lower mean across the investigated groups. The 45 mm/min group contains three ND sections among nine conditions, whereas the 36 mm/min group contains one among eleven. The assigned zeros are included in these means and support the favorable pooled result at 45 mm/min.

5.3. Rotational speed and heat generation

Rotation supplies both frictional interaction at tool–material contacts and deformation within the stirred region. Increasing angular speed increases mechanical power and can promote softening and stronger tool-driven transport. However, torque and contact conditions themselves change as the alloy softens. Heat generation therefore depends on the coupled sliding, sticking, and deformation conditions rather than rotational speed alone [17]. Effective consolidation requires sufficient mobility to refill the tool wake while retaining enough confinement for closure. Greater rotation can assist one tool profile yet alter the balance unfavorably for another.

The pooled mean area is 0.382 mm² at 2000 rpm and 0.757 mm² at 3150 rpm. The lower rotation level gives an approximately 49.5% lower mean across the examined groups. Both groups contain two ND sections. This comparison supports 2000 rpm as the more favorable pooled rotation level within the investigated conditions.

5.4. Pin length and interlayer engagement

Pin length affects the depth over which tool contact, deformation, and material exchange act beneath the shoulder. Because each added sheet is nominally 1.6 mm thick, both tested lengths are intended to engage material below the newly added sheet, with the 3 mm pin extending further into the underlying assembly. Actual engagement also depends on plunge and shoulder contact. A longer pin can strengthen subsurface stirring and interlayer exchange, but the benefit depends on the profile and the way displaced material is redistributed during closure. Length is consequently part of the flow configuration rather than an independent quality setting.

The pooled mean area is 0.552 mm² for 2 mm pins and 0.633 mm² for 3 mm pins with ND = 0. The 2 mm group gives an approximately 12.9% lower mean and contains three ND sections among eleven conditions, compared with one among nine for the 3 mm group. These results favor 2 mm pins at the group level under the selected criterion.

5.5. Coupled flow and thermal interpretation

The profile-dependent responses support a coupled interpretation of FSAM consolidation. Shoulder contact and pin geometry control where energy is introduced and how softened material is transported; traverse speed determines the duration of this interaction, and pin length determines its depth. Threads can support axial exchange, cylindrical pins maintain a more uniform radius along their body, and tapered pins change the local surface velocity and contact geometry with depth. These distinctions help explain why tools operating at the same nominal speeds do not leave the same discontinuity morphology.

The thermal cycles also matter for heat-treatable AA7075: repeated stirring and reheating can alter the microstructural state of successive layers, as discussed in FSAM process–microstructure studies [11, 12]. Here, the directly assessed response is visible interlayer discontinuity area. The favorable conditions therefore identify successful macroscopic closure in the examined sections. The observed area changes show that the response varies with the combination of geometry, speed, and engagement. The proposed flow and thermal mechanisms provide a physical interpretation of these differences.

5.6. Favorable processing combinations

Samples 8, 15, 19, and 20 are tied at an assigned area of 0.00 mm² under ND = 0 (Table 4). The threaded 2 mm pin at 45 mm/min is a particularly useful starting configuration because both 2000 and 3150 rpm give ND sections (samples 19 and 20). This outcome is consistent with effective helical material exchange combined with

sufficient interlayer engagement under the shorter residence time. The conical 2 mm pin at 3150 rpm and 45 mm/min and the cylindrical 3 mm pin at 2000 rpm and 36 mm/min provide alternative successful combinations.

Sample	Pin geometry	Rotation (rpm)	Traverse (mm/min)	Pin length (mm)	Discontinuity area (mm^2, ND = 0)
8	Conical	3150	45	2	0.00 (ND)
15	Cylindrical	2000	36	3	0.00 (ND)
19	Threaded	2000	45	2	0.00 (ND)
20	Threaded	3150	45	2	0.00 (ND)

Table 4. Tested combinations with no clearly resolved macroscopic discontinuity; area is assigned zero under ND = 0.

Sample 19 is a practical initial setting for subsequent builds because it combines the favorable threaded profile and 45 mm/min travel with the lower rotation level. Sample 20 is equally favorable under the visible discontinuity-area criterion and provides a higher-rotation comparison. Their selection follows the observed section quality; the proposed thermal and flow explanation should be evaluated together with interlayer microstructure and mechanical performance as the process is developed.

6. Conclusion

Three-layer AA7075 assemblies were produced through two successive FSAM joining stages. The examined sections lead to the following conclusions:

1. Pin geometry was associated with different macroscopic discontinuity patterns under the tested conditions. The threaded group had the lowest mean discontinuity area, 0.334 mm^2. Helical contact offers a plausible route for enhanced exchange across the interface, while the cylindrical and conical pins impose different deformation fields along their engaged depth.

2. The pooled mean area was 0.382 mm^2 at 2000 rpm, compared with 0.757 mm^2 at 3150 rpm, indicating an approximately 49.5% reduction at the lower rotational speed across the examined groups.

3. The pooled mean area decreased from 0.642 mm^2 at 36 mm/min to 0.523 mm^2 at 45 mm/min, representing an approximately 18.5% reduction with increasing traverse speed across the investigated groups.

4. Samples 8, 15, 19, and 20 are tied at zero. Threaded 2 mm pins at 45 mm/min produced ND sections at both rotation levels and are favorable candidates for continued process development, with 2000 rpm a practical starting setting.

Funding

This research was supported by the Iran National Science Foundation (INSF) under grant No. 40501063.

References

[1] M. Akbari, A. Heidarzadeh, E. Hassanzadeh. Friction stir welding and friction stir processing of additively manufactured components: A comprehensive review. *Journal of Materials Research and Technology* 43 (2026) 5137–5166. https://doi.org/10.1016/j.jmrt.2026.07.092

[2] M. Akbari, M.A. Kazemi, A. Moghanian, E. Hassanzadeh. A comprehensive review of friction stir lap welding. *Results in Engineering* 30 (2026) 109789. https://doi.org/10.1016/j.rineng.2026.109789

[3] A. Hassan, S.R. Pedapati, M. Awang, I.A. Soomro. A comprehensive review of friction stir additive manufacturing (FSAM) of non-ferrous alloys. *Materials* 16(7) (2023) 2723. https://doi.org/10.3390/ma16072723

[4] K.N. Nouranga, B.N. Prashanth, T. Ram Prabhu. A comprehensive review of solid-phase additive techniques: Insights into friction stir additive manufacturing (FSAM) and additive friction stir deposition (AFSD). *Results in Engineering* 27 (2025) 106604. https://doi.org/10.1016/j.rineng.2025.106604

[5] K.K. Jha, R. Kesharwani, M. Imam. Microstructure, texture, and mechanical properties correlation of AA5083/AA6061/SiC composite fabricated by FSAM process. *Materials Chemistry and Physics* 296 (2023) 127210. https://doi.org/10.1016/j.matchemphys.2022.127210

[6] K.K. Jha, R. Kesharwani, M. Imam. Microstructure and mechanical properties correlation of FSAM employed AA5083/AA7075 joints. *Transactions of the Indian Institute of Metals* 76(2) (2023) 323–333. https://doi.org/10.1007/s12666-022-02672-9

[7] M. Akbari, T. DebRoy, P. Asadi, T. Sadowski. Recent advances in friction stir welding/processing tools. *Journal of Manufacturing Processes* 142 (2025) 99–156. https://doi.org/10.1016/j.jmapro.2025.03.089

[8] R.S. Mishra, R.S. Haridas, P. Agrawal. Friction stir-based additive manufacturing. *Science and Technology of Welding and Joining* 27(3) (2022) 141–165. https://doi.org/10.1080/13621718.2022.2027663

[9] S. Palanivel, P. Nelaturu, B. Glass, R.S. Mishra. Friction stir additive manufacturing for high structural performance through microstructural control in an Mg based WE43 alloy. *Materials & Design* 65 (2015) 934–952. https://doi.org/10.1016/j.matdes.2014.09.082

[10] Y. Mao, L. Ke, C. Huang, F. Liu, Q. Liu. Formation characteristic, microstructure, and mechanical performances of aluminum-based components by friction stir additive manufacturing. *The International Journal of Advanced Manufacturing Technology* 83 (2016) 1637–1647. https://doi.org/10.1007/s00170-015-7695-9

[11] Z. Zhang, Z.-J. Tan, J.-Y. Li, Y.-F. Zu, J.-J. Sha. Integrated modeling of process–microstructure–property relations in friction stir additive manufacturing. *Acta Metallurgica Sinica (English Letters)* 33(1) (2020) 75–87. https://doi.org/10.1007/s40195-019-00945-9

[12] Y. Han, K. Lv, C. Lin, Y. Dai, X. Li, E. Wang. Sheet-based friction stir additive manufactured 6061 aluminium alloy: Microstructure, texture evolution and mechanical properties. *Materials Science and Engineering: A* 915 (2024) 147295. https://doi.org/10.1016/j.msea.2024.147295

[13] A. Hassan, M. Awang, S.R. Pedapati, K. Altaf, R.V. Marode, S.W. Ahmed. Experimental investigation on tool pin profile for defect-free multi-layered laminates using friction stir additive manufacturing. *Results in Engineering* 20 (2023) 101516. https://doi.org/10.1016/j.rineng.2023.101516

[14] A. Hassan, K. Altaf, M. Awang, S.R. Pedapati, N. Ahmed, R.V. Marode. Multi-objective optimization of friction stir additively manufactured Al-7075 multi-layered laminates. *Journal of Alloys and Compounds* 993 (2024) 174659. https://doi.org/10.1016/j.jallcom.2024.174659

[15] G. Girish. Analysis of microstructure and hardness of a double-layered AA7075 build developed by friction stir additive manufacturing. *Proceedings of the Institution of Mechanical Engineers, Part C: Journal of Mechanical Engineering Science* 239(9) (2025) 3334–3338. https://doi.org/10.1177/09544062241312881

[16] M. Akbari, A. Abdollahzadeh, M. Esfandiar. A comprehensive review of material flow in FSW/FSP: Experimental insights and simulation perspectives. *Engineering Reports* 7(4) (2025) e70138. https://doi.org/10.1002/eng2.70138

[17] H.N.B. Schmidt, J. Hattel, J. Wert. An analytical model for the heat generation in friction stir welding. *Modelling and Simulation in Materials Science and Engineering* 12(1) (2004) 143–157. https://doi.org/10.1088/0965-0393/12/1/013